Zhuang *et al. Energy Mater.* **2025**, *5*, 500015
DOI: 10.20517/energymater.2024.90

Energy Materials

Article

Open Access

Check for updates

High-performance novel anode-supported microtubular protonic ceramic fuel cells via highly efficient and simplified extrusion technology

Zichen Zhuang[1], Zuzhi Huang[2], Xiaoyu Zhang[1], Kui Liu[1], Guozhu Zheng[1], Ting Chen[1,*], Ruili Sun[1], Lang Xu[1], Shaorong Wang[1,*]

[1]School of Chemical Engineering & Technology, China University of Mining and Technology, Xuzhou 221116, Jiangsu, China.
[2]Jiangxi Key Laboratory of Surface Engineering, School of Materials and Energy, Jiangxi Science and Technology Normal University, Nanchang 330013, Jiangxi, China.

***Correspondence to:** Dr. Ting Chen, School of Chemical Engineering & Technology, China University of Mining and Technology, 1 Daxue Road, Xuzhou 221116, Jiangsu, China. E-mail: chenting@cumt.edu.cn; Prof. Shaorong Wang, School of Chemical Engineering & Technology, China University of Mining and Technology, 1 Daxue Road, Xuzhou 221116, Jiangsu, China. E-mail: srwang@cumt.edu.cn

How to cite this article: Zhuang, Z.; Huang, Z.; Zhang, X.; Liu, K.; Zheng, G.; Chen, T.; Sun, R.; Xu, L.; Wang, S. High-performance novel anode-supported microtubular protonic ceramic fuel cells via highly efficient and simplified extrusion technology. *Energy Mater.* **2025**, *5*, 500015. https://dx.doi.org/10.20517/energymater.2024.90

Received: 26 Jul 2024 **First Decision:** 2 Sep 2024 **Revised:** 23 Sep 2024 **Accepted:** 10 Oct 2024 **Published:** 9 Jan 2025

Academic Editors: Sining Yun, Jose A. Alonso **Copy Editor:** Fangling Lan **Production Editor:** Fangling Lan

Abstract

Protonic ceramic fuel cells (PCFCs) are regarded as efficient energy conversion devices for addressing the challenges of carbon neutrality, which can directly convert the chemical fuel energy into electricity at reduced operating temperatures below 700 °C. However, the insufficient strength and immature preparation processes of PCFCs limit their practical application. In this work, the novel anode-supported microtubular PCFCs with a tube diameter of less than 5 mm were successfully prepared by extrusion technology combined with a dip-coating method. The newly developed $BaZr_{0.4}Ce_{0.4}Y_{0.1}Gd_{0.1}O_{3-\delta}$ (BZCYG4411) proton-conducting electrolyte was synthesized using an extremely simple and efficient one-step solid-state reaction method, showing comparable electrical conductivity with $BaZr_{0.4}Ce_{0.4}Y_{0.1}Yb_{0.1}O_{3-\delta}$ (BZCYYb4411) and $BaZr_{0.1}Ce_{0.7}Y_{0.1}Yb_{0.1}O_{3-\delta}$ (BZCYYb1711) electrolytes, as well as excellent chemical stability. The single cell with $Ba_2Sc_{0.1}Nb_{0.1}Co_{1.5}Fe_{0.3}O_{6-\delta}$ (BSNCF) cathode exhibited a high peak power density of 906.86 mW cm^{-2} at 700 °C. Additionally, this microtubular PCFC demonstrated excellent stability after about 103 h durability test at a constant current of 0.5 A cm^{-2} at 650 °C. This study provides a highly efficient and simplified technology for fabricating high-performance and durable anode-supported microtubular PCFCs.

Keywords: BZCYG4411 proton-conducting oxide, new anode support, microtubular PCFC, large-length, extrusion

© The Author(s) 2025. **Open Access** This article is licensed under a Creative Commons Attribution 4.0 International License (https://creativecommons.org/licenses/by/4.0/), which permits unrestricted use, sharing, adaptation, distribution and reproduction in any medium or format, for any purpose, even commercially, as long as you give appropriate credit to the original author(s) and the source, provide a link to the Creative Commons license, and indicate if changes were made.

INTRODUCTION

Energy and environmental issues have become increasingly prominent in recent years[1]. Developing highly efficient, sustainable, and clean technologies is a top priority to achieve the goals of carbon neutrality and sustainable development. Compared to conventional coal-based thermal power generation technology, fuel cells are power generators that can convert the chemical energy in the fuels directly into electricity through electrochemical reactions. Unlike conventional systems limited by the Carnot cycle, fuel cells can achieve high energy conversion efficiency[2]. Among all fuel cell systems, solid oxide fuel cells (SOFCs) are the most promising electrochemical conversion devices due to their high efficiency, reliance on non-precious metal catalyst, and all-solid-state structure[3,4]. SOFCs generally can be divided into two categories according to the mobile carriers. The first one is oxygen ion-conducting SOFCs (called O-SOFCs), and the second one is proton-conducting ceramic fuel cells [named H-SOFCs or protonic ceramic fuel cells (PCFCs)][5]. Yttrium-stabilized zirconia (YSZ) and scandium-stabilized zirconia (SSZ) are the commonly used oxygen ion-conducting electrolytes for O-SOFCs. They have a higher activation energy (E_a, ~0.9 eV) for oxygen ion conduction and typically operate at a higher temperature (700-1,000 °C), owning to the larger ionic radius of the oxygen ions[6,7]. In contrast, the carrier of PCFCs, proton (H^+), has a much smaller radius and needs lower E_a (0.3~0.5 eV), making it possible to operate at low temperatures (< 700 °C)[8]. A lower operating temperature can effectively reduce the cost of accessory materials and improve the thermo-mechanical stability of the cell. In addition, water is generated on the cathode side of PCFCs, which helps to avoid the fuel dilution and improves the fuel utility[9-11].

To date, both planar and tubular PCFCs have been widely investigated and significant improvements reported[12]. Compared to planar PCFCs, tubular PCFCs have been receiving increasing attention because of their advantages of high mechanical strength, fast start-up, easy sealing, and good thermal cycle stability[13]. However, tubular PCFCs typically exhibit low power density due to the elongated current path, which increases the internal resistance[14]. The microtubular structure combines the advantages of both tubular and planar, featuring a smaller tube radius and shorter current channels, effectively reducing the loss for current collection and transmission, ultimately enhancing cell performance[15,16]. At the same time, the smaller size minimizes the impact of stresses from thermal gradients, allowing for rapid start-up, better mechanical strength, and low thermal shock damage[17]. However, most existing research has been focused on planar PCFCs, while there is little information available on developing microtubular PCFCs.

For the fabrication of anode functional layer (AFL) and electrolyte layer of microtubular PCFCs, the dip-coating method is one of the most commonly used techniques, which only requires one to three dip-coating cycles to achieve the desired thickness (10-30 μm). However, for the anode supports, which play a critical role in supporting the whole cell structure, it need to reach a certain thickness of around hundred microns. Currently, several techniques have been used for the thick anode support fabrication of microtubular PCFCs, such as phase inversion, dip-coating, and 3D printing. Hou *et al.* fabricated a high-performance microtubular PCFC with an outer cell diameter of 0.38 mm via phase inversion method (support layer) combined with a dip-coating process (electrolyte layer), achieving a maximum power density of 2.62 W cm^{-2} at 700 °C[18]. Tong *et al.* also developed a phase inversion method for the batch preparation of microtubular PCFCs with an extremely small outer diameter of 0.15 mm, showing a maximum power density of 601.2 mW cm^{-2} at 700 °C[19]. The phase inversion method can prepare electrode supports with an open-straight pore structure, which facilitates gas transfer and improves electrochemical performance. However, the large open-straight pore structure PCFCs may have insufficient strength, even in the microtubular structure, limiting its large-scale practical application[20]. The dip-coating was also widely used for the preparation of microtubular PCFCs. Chen *et al.* prepared a microtubular PCFC with an outer diameter of

5 mm using the dip-coating method, with a peak power density (PPD) of 810 mW cm^{-2} at 700 °C[21]. Although the dip-coating method is simple and inexpensive to prepare anode supports, it is highly inefficient and unsuitable for large-scale preparation because repeated dip-coating is required to achieve a certain thickness, similar to the slip-casting[22]. Zou *et al.* reported a 3D-printed tubular PCFC with an efficient area of 12.5 cm^2 and a total power output of 2.45 W at 650 °C[23]. However, the cost of the 3D printing equipment is excessively high[24]. Compared to the aforementioned methods for tubular PCFCs, the extrusion technology is currently one of the most effective methods for preparing tubular cells due to its economic feasibility, intuitively simple operation, extremely high efficiency, and the ability to prepare tubular cells of any length and diameter. Nevertheless, the extrusion technology has not been utilized for the preparation of microtubular PCFCs[25,26].

The commonly used proton-conducting electrolytes, such as $BaZr_{0.1}Ce_{0.7}Y_{0.2}O_{3-\delta}$ (BZCY), $BaZr_{0.4}Ce_{0.4}Y_{0.1}Yb_{0.1}O_{3-\delta}$ (BZCYYb4411), and $BaZr_{0.1}Ce_{0.7}Y_{0.1}Yb_{0.1}O_{3-\delta}$ (BZCYYb1711), have been extensively investigated. The commonly used synthesis methods are the sol-gel or the conventional solid-state reaction (SSR) method[27-29]. The sol-gel method is not suitable for large-scale preparation due to the complexity of fabrication process and the uncertainty of crystallization water in nitrates. The conventional SSR method, which uses metal oxides as raw materials, is simple but requires multiple rounds of ball-milling and calcination. Moreover, the incorporation of trivalent rare-earth metal ions into the crystal lattice is challenging, leading to the formation of heterogeneous phases. These drawbacks hinder the large-scale application of the conventional SSR[30].

In this work, a novel $BaZr_{0.4}Ce_{0.4}Y_{0.1}Gd_{0.1}O_{3-\delta}$ (BZCYG4411) electrolyte was synthesized using an extremely simple and efficient novel one-step SSR method with raw materials including $BaCO_3$, $Ce_{0.8}Gd_{0.2}O_{2-\delta}$ (GDC20), 8 mol% Y_2O_3 stabilized ZrO_2 (8YSZ), and Y_2O_3. This one-step SSR method requires only a single ball-milling and calcination to obtain the pure phase compared to conventional SSR. A microtubular PCFC (a tube diameter of less than 5 mm) with the configuration of NiO-BZCYG4411 anode support|NiO-BZCYYb1711 AFL|BZCYYb1711 electrolyte layer|$Ba_2Sc_{0.1}Nb_{0.1}Co_{1.5}Fe_{0.3}O_{6-\delta}$ (BSNCF) cathode was successfully prepared using a simple and efficient extrusion technology combined with a dip-coating method. BSNCF oxide was selected as the cathode due to its low thermal expansion coefficient (TEC), which has not been applied in tubular PCFCs. The cell achieved high PPDs of 906.86 and 655.56 mW cm^{-2} at 700 and 650 °C, respectively. Moreover, the microtubular PCFCs demonstrated favorable stability after about 103 h durability test at a constant current of 0.5 A cm^{-2} at 650 °C. This newly developed fabrication method for BZCYG4411, along with extrusion technology for cell preparation, provides a simple, economical, and efficient way to fabricate large-scale microtubular PCFCs.

EXPERIMENTAL

Synthesis of electrolyte and cathode powders

The BZCYG4411 oxide was synthesized using a one-step SSR method using two types of raw materials. For type 1, $BaCO_3$ (Shanghai Aladdin Biochemical Technology Co., Ltd., 99.95%, China), GDC20 (Ruier Powder Materials Corporation, China), 8YSZ (Sinocera, China), and Y_2O_3 (Aladdin, 99.99%, China) were weighed and mixed according to the stoichiometric ratio, followed by ball-milling in ethanol for 24 h at 300 r/min. Then the mixture was completely dried at 80 °C in an oven. Subsequently, the dry powder was pressed into large pellets at 10 MPa with a diameter of 20 mm and then calcined at 1,200 °C for 12 h to obtain pure BZCYG4411 [Figure 1]. The reaction equation is given in

$$BaCO_3 + GDC20 + 8YSZ + Y_2O_3 \rightarrow BZCYG4411 \quad (1)$$

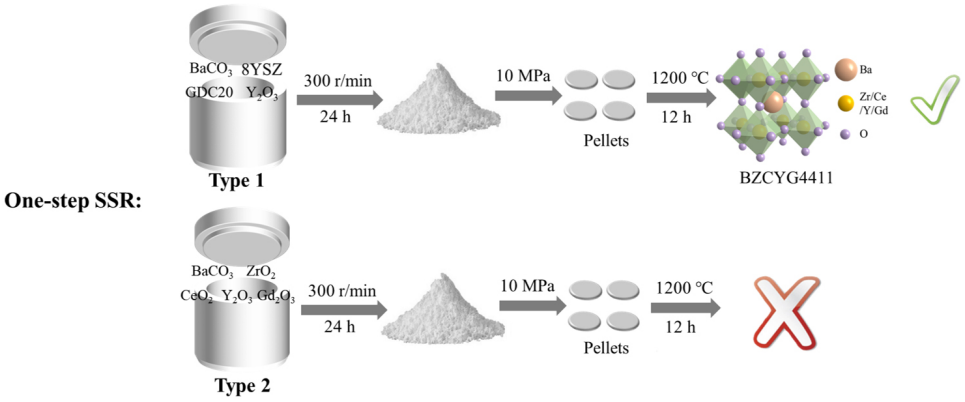

Figure 1. Schematic diagram of the synthesis process of BZCYG4411 powder using one-step SSR method with two types of raw materials.

For type 2, the same one-step SSR synthesis method was adopted using the raw materials of $BaCO_3$, ZrO_2 (Aladdin, 99%, China), CeO_2 (Aladdin, 99.99%, China), Y_2O_3, and Gd_2O_3 (Aladdin, 99.99%, China). Meanwhile, dense bars of BCZYG4411 were prepared by dry-pressing at the pressure of 200 MPa and sintered at 1,250 °C for 5 h, which were used for the electrical conductivity, TEC, and linear shrinkage test. For comparison, the commercial BZCYYb4411 (Ruier Powder Materials Corporation, China) was also sintered at 1,100 °C for 10 h for achieving the desirable crystallinity.

The BSNCF oxide was synthesized using a conventional SSR method. The stoichiometric amounts of $BaCO_3$, Sc_2O_3 (Aladdin, 99.9%, China), Nb_2O_5 (Aladdin, 99.99%, China), and Fe_2O_3 (Aladdin, 99%, China) powders were mixed and ball-milled in ethanol for 24 h at 400 r/min. Then the mixed powder was dried, crushed, and calcined at 1,150 °C for 20 h to obtain pure BSNCF[31,32]. Additionally, the commonly used $PrBa_{0.5}Sr_{0.5}Co_{1.5}Fe_{0.5}O_{6-\delta}$ (PBSCF) cathode was also used for the performance comparison. The synthesis method can be observed in our previous work[20].

Preparation of anode-supported tubes by extrusion

The above synthesized BZCYG4411 (type 1) powder, nickel oxide (NiO, J.T. Baker, USA), the pore-forming material of polymethyl methacrylate (PMMA, Aladdin, China), and ethanol were mixed in a mass ratio of 4:6:1:11 and ball-milled for 48 h at 300 r/min to obtain a well-dispersed mixed slurry. The slurry was then dried at 80 °C to obtain the mixed powder for extrusion. Next, 1 kg of the primary anode support powder, 30 g of binder hydroxypropyl methylcellulose (HPMC, Aladdin, China), 20 g of plasticizer dioctyl phthalate (DOP, Shanghai Sinopharm, AR, China), 15 g of lubricant tung oil (Aladdin, China), 20 g of dispersant triethanolamine (TEA, Shanghai Sinopharm, AR, China), pH neutralizer 30 wt% aqueous citric acid solution (Aladdin, 99.5%, China), and 200 g of deionized water were mixed in a powder kneader in turn for 5 h to obtain a homogenous mixture with adequate stickiness, plasticity, and pH-neutrality[33,34]. The mixed mud was taken out and sealed using cling film and a sealed bag to prevent exposure to air. It was then placed in a low-temperature, dark-location place for two days to undergo aging and obtain the desirable mixed mud for extrusion.

The anode-supported tubes of the microtubular cells were prepared using the extrusion method, as shown in Figure 2. The mixed mud was fed into the extrusion machine, with the extrusion rate at 0.5 cm s^{-1} by adjusting the rotational speeds of the upper and lower shaft motors. Before extrusion, the mixed mud was vacuum treated in the machine to remove any air bubbles. The extruded anode-supported tubes were dried in an oven at 50 °C to remove moisture.

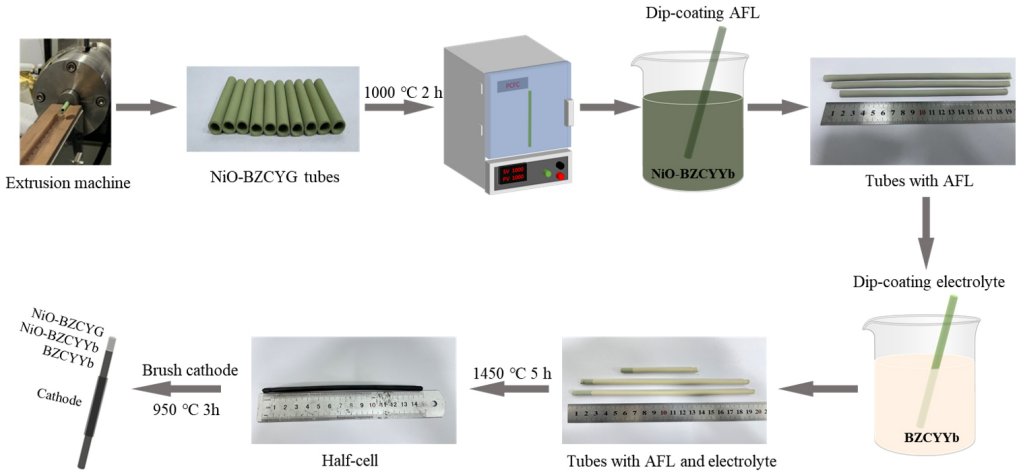

Figure 2. Schematic preparation process of microtubular PCFCs.

Preparation of microtubular PCFCs

The schematic drawing illustrating the preparation process of microtubular PCFCs is presented in Figure 2. Firstly, the NiO-BZCYG4411 tubes were calcined at 1,000 °C for 2 h to remove the organic solvents. Secondly, the AFL slurry was prepared by ball-milling 10 g of NiO, 10 g of commercial BZCYYb1711 (Ruier Powder Materials Corporation, China), and 0.6 g of polyvinyl pyrrolidone (PVP, K30, Aladdin, China) in 70 g of ethanol for 12 h at 400 r/min. The electrolyte layer slurry was prepared using the same ball-milling method, combining 20 g of BZCYYb1711, 0.1 g of NiO (sintering additive), 0.6 g of PVP, and 75 g of ethanol. Both slurries were transferred to beakers and placed in a vacuum defoamer to remove the air before the dip-coating process[35]. Since the anode-supported tubes are open at both ends, one end was sealed with paraffin to prevent the slurry from entering the inner during the dip-coating process. Thirdly, the tubes were dip-coated in the AFL slurry of NiO-BZCYYb1711 for 15 s and dried naturally in the air. Finally, the BZCYYb1711 electrolyte layer was prepared using the same method with two rounds of dip-coating, followed by co-sintering at 1,450 °C for 5 h to obtain the half-cell. The length of the half-cell was approximately 15 cm, and the out diameter was about 0.48 cm.

The BSNCF/PBSCF cathode slurry was prepared by mixing an equal mass of 5 wt% ethyl cellulose-terpineol solution (Shanghai Sinopharm, AR, China), which was then milled for 12 h. The cathode slurry was applied to the surface of the BZCYYb1711 electrolyte and dried at 80 °C in an oven, followed by sintering at 950 °C for 3 h to obtain the full microtubular PCFCs.

Electrochemical performance test

The fabricated microtubular PCFCs were cut into smaller pieces (about 2 cm) with an effective cathode area of 0.7 cm^2. The open circuit voltage (OCV), current-voltage-power (I-V-P) and electrochemical impedance spectra (EIS) curves of microtubular PCFCs were examined using the electrochemical workstation (BioLogic SP-300, France). The cell was tested with 3% humidified H_2 (40 mL/min) as the fuel and ambient air as the oxidant. The frequency range was set from 0.1 Hz to 100 kHz with a 10 mV AC signal. The surfaces of the anode and cathode were connected with silver wires using a silver paste (DAD-87) respectively to collect current. A ceramic adhesive (Ceramabond 552, Aremco Products Inc.) was used for sealing the microtubular PCFCs.

Characterization

The phase structure of the electrolyte and cathode powders was characterized by X-ray diffraction (XRD, Bruker D8 Advance, Germany). The high-resolution image, diffraction pattern, and element distribution of BZCYG4411 powder was characterized using high-resolution transmission electron microscopy (HR-TEM, FEI talos F200x G2, USA) equipped with energy-dispersive X-ray (EDX) mapping. The powder of BZCYG4411 and the surface and cross-sectional microstructure of microtubular PCFCs were observed using field scanning electron microscopy (FSEM, TESCAN MAIA3 LMH, Czech). The electrical conductivity of BZCYG4411 was measured by four-probe direct current (DC) method from 500 to 700 °C using the electrochemical workstation. The TEC and linear shrinkage of samples were evaluated in ambient air using the dilatometer (DIL 402 C, NETZSCH).

RESULTS AND DISCUSSION

Characterization of electrolytes and cathode

Figure 3A presents the XRD patterns of BZCYG4411 oxide (type 1) prepared by the one-step SSR method and commercial BZCYYb4411 oxide. The BZCYYG4411 exhibits eight broad peaks at 29.25°, 36.00°, 41.85°, 51.89°, 60.71°, 68.86°, 76.49°, and 83.96°, corresponding to the (110), (111), (200), (211), (220), (310), (222), and (321) crystal planes, respectively. These peaks matched well with the BZCYY4411 oxide and $BaZr_{0.4}Ce_{0.4}Y_{0.2}O_{2.89}$ (PDF#01-090-2002) oxide. No impurity phases were observed. In contrast, the BZCYG4411 synthesized using metal oxide as raw materials (type 2) shows several additional oxide peaks, as shown in Supplementary Figure 1. Therefore, the type 1 of BZCYG4411 was used for further investigation. Figure 3B illustrates the XRD refinement of BZCYG4411 (type 1) with lattice parameters of a = 6.08 Å, b = 8.61 Å, c = 6.11 Å (Space group: *Imma*, R_p = 7.92%, R_{wp} = 10.57%, GOF = 1.28, Supplementary Table 1). Supplementary Figure 2 shows the scanning electron microscopy (SEM) image of the BZCYG4411 powder and EDX mapping results, indicating that the synthesized powder elements are extremely homogeneous. The high resolution-transmission electron microscopy (HR-TEM) image is shown in Figure 3C, revealing a lattice spacing of 0.150 nm, corresponding to the (220) crystal plane. The elemental distribution of BZCYG4411 was further investigated using high-angle annular dark field scanning transmission electron microscopy (HAADF-STEM) coupled with EDX mapping results. The Ba, Zr, Ce, Y, Gd, and O elements were uniformly distributed, with the atomic ratios closely matching the theoretical stoichiometric values, as shown in Figure 3D. These results demonstrate an effective and cost-efficient method for synthesizing BZCYG4411 using a simple one-step SSR method, with $BaCO_3$, GDC20, 8YSZ, and Y_2O_3 as raw materials. In order to further confirm the chemical and structure stability of BZCYG4411 electrolyte, the BZCYG4411 pellet was heat treated in 10% H_2O-90% N_2 and 3% CO_2-97% N_2 at 650 °C for 50 h, respectively. Supplementary Figure 3 displays the XRD patterns of BZCYG4411 after the treatment, showing that no impurity peak was generated. These results indicate that BZCYG4411 can maintain good chemical and structure stability in both H_2O and CO_2 atmospheres.

Figure 4A shows the electrical conductivity of BZCYG4411 measured by four-probe DC method at 500-700 °C in both dry and wet air (3 vol% H_2O). The electrical conductivity increases gradually with temperature from 500 to 700 °C, exhibiting p-type semi-conducting behavior[36]. The BZCYG4411 oxide exhibited higher conductivity in wet air compared to dry air, which is attributed to the increased proton concentration resulting from the hydration reaction. Meanwhile, it can be seen that the BZCYG4411 shows comparable conductivity in both wet and dry air conditions to that of commonly used proton-conducting electrolytes, such as BZCYYb4411, $BaZr_{0.3}Ce_{0.5}Y_{0.1}Yb_{0.1}O_{3-\delta}$ (BZCYYb3511), and BZCYYb1711[28,36,37], making it a viable candidate for application in PCFCs. The E_a of an electrolyte can be defined as the energy barrier that internal carriers must overcome to facilitate their movement and conduction within the electrolyte, thereby enabling the electrochemical reaction to occur[38]. Figure 4B shows the Arrhenius plots of conductivity of BZCYG4411 oxide. The E_a of 0.43 eV in wet air is lower than 0.48 eV in dry air, further

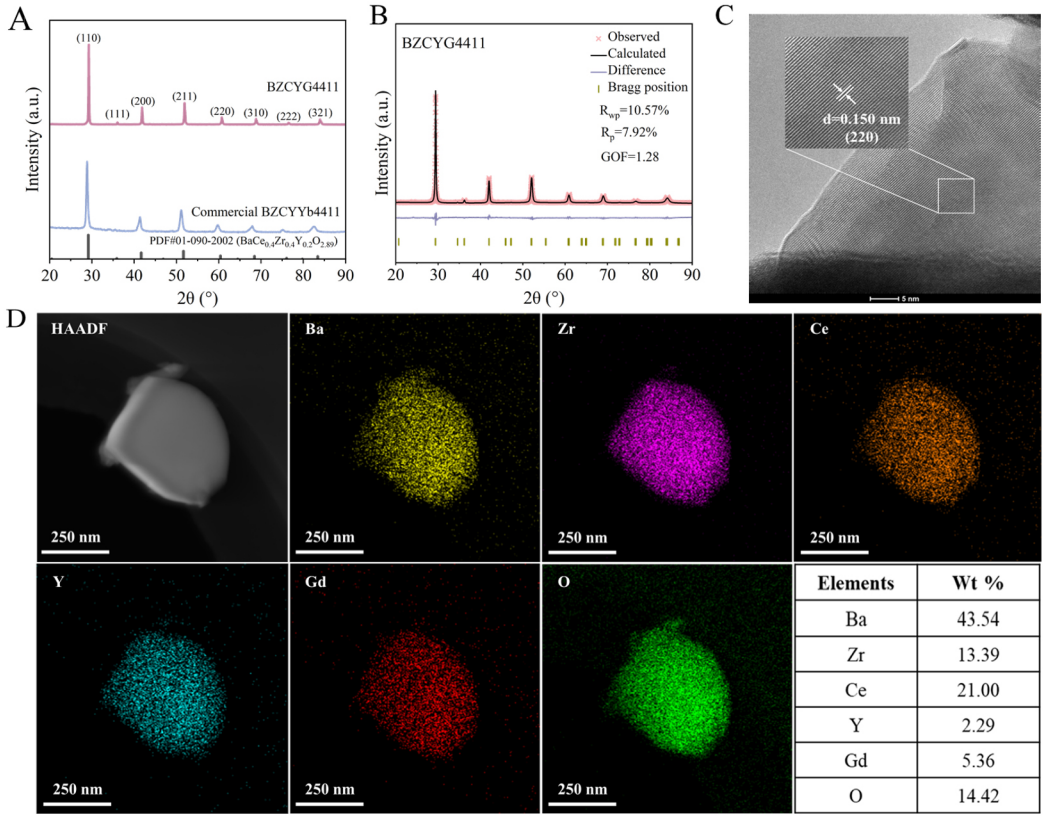

Elements	Wt %
Ba	43.54
Zr	13.39
Ce	21.00
Y	2.29
Gd	5.36
O	14.42

Figure 3. (A) XRD patterns of BZCYG4411 and commercial BZCYYb4411; (B) Rietveld refinement profiles of BZCYG4411; (C) HR-TEM image and (D) EDX mapping results of BZCYG4411.

proving the hydration capacity. This low E_a also confirmed the characteristic behavior for proton conductors[39,40]. To further investigate the contributions of electronic and ionic to the total conductivity, electrical conductivity measurement of BZCYG4411 was performed under dry N_2 conditions, as shown in Supplementary Figure 4A. BZCYG4411 exhibits exclusively electronic conductivity under dry N_2 conditions, whereas it exhibits mixed conductivity of H^+, O^{2-}, and e^- under humid air conditions. The transference number (t) for ions and electrons was calculated using

$$t_{ion/electrn} = \frac{\sigma_{ion/electron}}{\sigma_{ion} + \sigma_{electron}} \quad (2)$$

where σ_{ion} is ionic conductivity and $\sigma_{electron}$ is the electronic conductivity. The calculated transference numbers are displayed in Supplementary Figure 4B, showing a gradual decrease in ionic conductivity and a corresponding increase in electronic conductivity as the temperature rises.

In order to ensure the effectiveness of the sintering procedure, the thermal behavior of BZCYG4411 and NiO-BZCYG4411 (6:4) dense bars was also evaluated. The TECs of NiO-BZCYG4411 anode support and BZCYG4411 measured from room temperature to 1,000 °C are shown in Figure 4C. The average TEC of BZCYG4411 is 10.64 × 10^{-6} K^{-1}, which is similar to that of BZCYYb1711[41]. The average TEC of NiO-BZCYG4411 anode support is 11.03 × 10^{-6} K^{-1}, which is also comparable with the protonic electrolytes. This compatibility helps avoid separation or cracking during the co-sintering process of the cells. Additionally, the sintering shrinkage behavior of NiO-BZCYG4411 anode support and BZCYG4411 electrolyte is

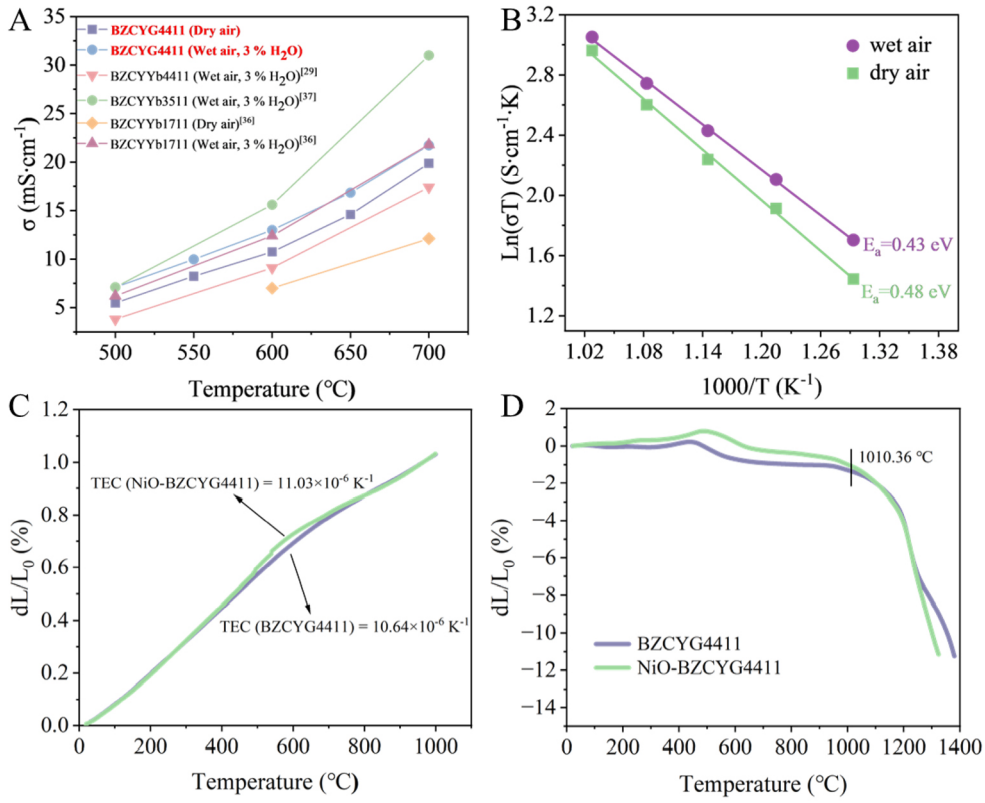

Figure 4. (A) The electrical conductivity comparison of BZCYG4411 and other reported electrolytes; (B) Arrhenius plots of electrical conductivity of BZCYG4411 measured at 500-700 °C; (C) The TECs of BZCYG4411 and NiO-BZCYG4411 anode support measured at room temperature to 1,000 °C; (D) The linear shrinkages of the BZCYG4411 and NiO-BZCYG4411 versus temperature.

presented in Figure 4D. They both had a smaller degree of shrinkage until 1,010.36 °C. The shrinkage of Ni-BZCYG4411 anode support occurs earlier than the shrinkage of BZCYYb1711 (at 1,155 °C), which may facilitate the densification of electrolyte[41,42].

The matched thermal properties between the electrolyte and cathode materials are the crucial factors influencing the thermal-mechanical stability of PCFCs. Considering the special structure of microtubular PCFCs, the matching of thermal properties becomes more important, so a new low thermal expansion material, BSNCF oxides, was selected. Figure 5A shows the XRD pattern of BSNCF obtained using the SSR method and sintered at 1,150 °C for 20 h, indicating a pure phase with a typical double-perovskite crystal structure. Figure 5B shows the TEC of BSNCF measured from room temperature to 1,000 °C. The TEC value of BSNCF is 13.9 × 10^{-6} K^{-1}, significantly lower than that of PBSCF oxide[43]. Figure 5C compares the TEC values of BZCYYb1711 and other Co-based or new cathode materials, such as $La_{0.6}Sr_{0.4}Co_{0.8}Fe_{0.2}O_{3-\delta}$ (LSCF, 21.4 ×10^{-6} K^{-1})[44], $Ba_{0.5}Sr_{0.5}Co_{0.8}Fe_{0.2}O_{3-\delta}$ (BSCF, 23.6 ×10^{-6} K^{-1})[45], $Ba_{0.95}La_{0.05}Fe_{0.8}Zn_{0.2}O_{3-\delta}$ (BLFZ, 20.1 × 10^{-6} K^{-1})[46], and $BaCo_{0.4}Fe_{0.4}Zr_{0.1}Y_{0.1}O_{3-\delta}$ (BCFZY, 21.6 × 10^{-6} K^{-1})[45]. It can be observed that all of the Co-based materials have higher TEC values than BZCYYb1711 (10.18 × 10^{-6} K^{-1}) electrolyte, whereas BSNCF has a TEC closer to that of BZCYYb1711, which may ensure better thermal compatibility in PCFCs[47].

Electrochemical performance and stability

Figure 6 summarizes the electrochemical performance and stability of the microtubular PCFC with BSNCF cathodes. The I-V-P curves of the single cell measured at different temperatures are shown in Figure 6A. The OCVs were 1.002, 1.040, and 1.085 V at 700, 650, and 600 °C, respectively, which are close to the

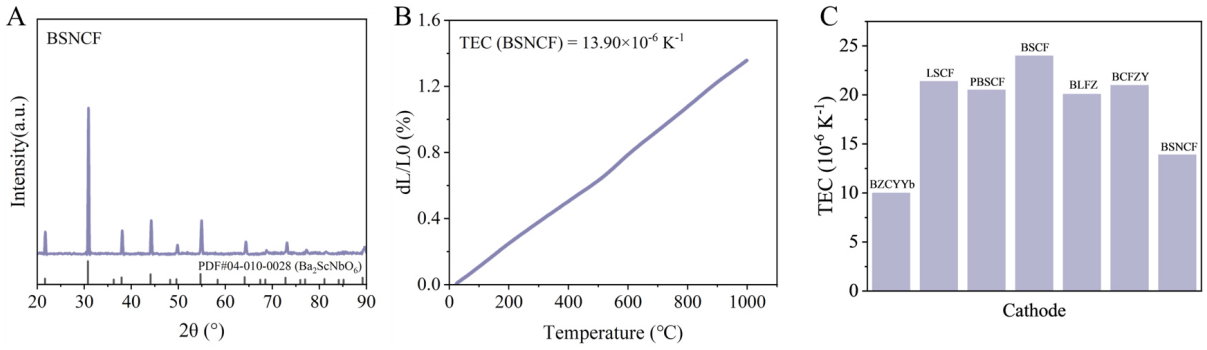

Figure 5. (A) XRD pattern of BSNCF; (B) The TEC of BSNCF measured at room temperature to 1,000 °C; (C) The TECs comparison of BZCYYb1711 electrolyte with other commonly used cathode materials.

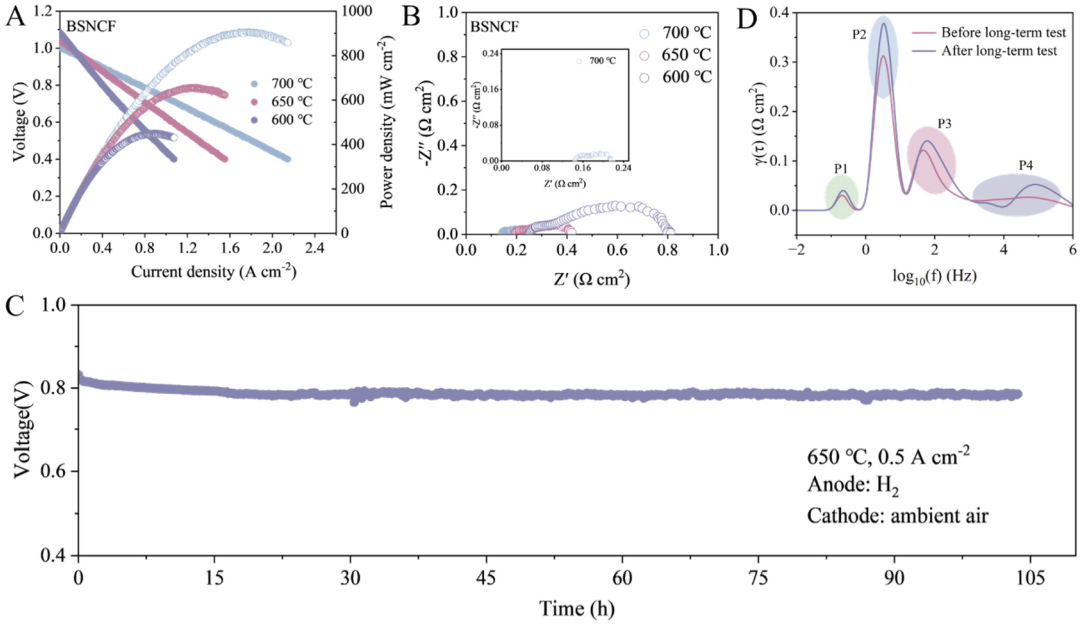

Figure 6. The electrochemical performance of the microtubular PCFC with BSNCF cathode. (A) I-V-P curves; (B) EIS curves; (C) Stability test at 650 °C; (D) DRT analysis of the cell before and after the durability test.

theoretical values, indicating that the electrolyte is dense[48]. The PPDs of 906.86, 655.56, and 449.94 mW cm^{-2} at 700, 650, and 600 °C were achieved, respectively, which are comparable to other reported tubular PCFCs prepared using the extrusion technology as shown in Table 1. The corresponding EIS curves under OCV are shown in Figure 6B. The ohmic resistance (R_o) of the cell was 0.14, 0.19, and 0.25 Ω cm^2 at 700, 650, and 600 °C, respectively, while the polarization resistance (R_p) was 0.07, 0.23, and 0.56 Ω cm^2, respectively. At 700 °C, the R_o was greater than the R_p, indicating that the cell performance was mainly affected by the electrolyte at 700 °C. To further evaluate the stability of a single cell, the measurement was conducted at 650 °C at a constant current of 0.5 A cm^{-2}, as shown in Figure 6C. The operating voltage decreased from 0.83 to 0.80 V during the initial 20 h of the test and remained relatively stable since then. This might be attributed to the fact that the water generated on the cathode side competes with oxygen for adsorption. The operating voltage will be stable when the competitive adsorption reaches dynamic equilibrium[49]. The total degradation rate was about 3.6% after 103 h of stability testing. Supplementary Figure 5A and B shows the I-V-P and EIS curves of the cell before and after the stability test.

Table 1. PPDs of tubular PCFCs via the extrusion technology

Outer diameter (mm)	Electrolyte (thickness)	Cathode	Temperature (°C)	PPDs (mW cm^{-2})	Ref.
8.2	BZCYYb (~15 μm)	BCFZY	600	517	[34]
8.2	BZCYYb (~15 μm)	BSCF	600	534	[34]
8.2	BZCYYb (~15 μm)	PBSCF	600	326	[34]
9.3	BZCY (~10 μm)	LSCF-BZCY	600	300	[26]
–	BZCYYb (~20 μm)	PNOF-BZCYYb	600	390	[54]
5.0	BZI	LSCF	600	143	[55]
4.8	BZCYYb (~15 μm)	BSNCF	600	449.94	This work
4.8	BZCYYb (~20 μm)	PBSCF	600	546.61	This work

BZCYYb: $BaZr_{0.1}Ce_{0.7}Y_{0.1}Yb_{0.1}O_{3-\delta}$; BCFZY: $BaCo_{0.4}Fe_{0.4}Zr_{0.1}Y_{0.1}O_{3-\delta}$; BSCF: $Ba_{0.5}Sr_{0.5}Co_{0.8}Fe_{0.2}O_{3-\delta}$; PBSCF: $PrBa_{0.5}Sr_{0.5}Co_{1.5}Fe_{0.5}O_{6-\delta}$; BZCY: $BaZr_{0.1}Ce_{0.7}Y_{0.2}O_{3-\delta}$; LSCF: $La_{0.6}Sr_{0.4}Co_{0.2}Fe_{0.8}O_{3-\delta}$; PNOF: $Pr_2NiO_{3.9+\delta}F_{0.1}$; BZI: $BaZr_{0.8}In_{0.2}O_{3-\delta}$

The PPD slightly decreased from 655.36 to 632.77 mW cm^{-2} at 650 °C, and the R_p increased from 0.23 to 0.24 Ω cm^2. No change was observed on the R_o.

To further understand the possible causes of degradation, the distribution of relaxation time (DRT) was used to analyze the EIS variations of the cell before and after the durability test. Figure 6D shows four typical DRT peaks from low to high frequencies, denoted as P1, P2, P3, and P4, which represent the four main steps in the electrode reaction process of the cells[50]. The P1 peak in the low-frequency region is mainly related to gas diffusion in the electrode of the cell, and the P2 peak in the mid-frequency region is closely related to the oxygen reduction reaction (ORR) and oxygen-ion transport at the three-phase-boundary (TPB) interface, whereas the P3 peak in the mid- to high-frequency region is related to the formation and diffusion of protons in the anode, and the P4 peak in the high-frequency region represents the process of electron transfer and ion transfer through the interface between the electrolyte and the electrode[51-53]. After the stability test, the P2-P4 peaks showed slight increases, indicating a deterioration in the ORR process, which may result from competition between the generated water and oxygen absorption as explained previously.

In addition, the electrochemical performance of microtubular PCFC with PBSCF cathode is also evaluated, as shown in Supplementary Figure 6A and B. The PPDs of 546.61 and 866.71 mW cm^{-2} were obtained at 600 and 650 °C, respectively. These results represent the highest performance compared to other previously reported tubular PCFCs fabricated by extrusion, as summarized in Table 1. The corresponding R_o were 0.28 and 0.22 Ω cm^2, respectively, and R_p were 0.16 and 0.07 Ω cm^2. Supplementary Figure 6C shows the good long-term stability of the cell under a constant current of 0.5 A cm^{-2} at 650 °C for 105 h, further confirming the good stability of microtubular PCFC prepared by extrusion technology. Meanwhile, the cell performance of tubular PCFC fabricated by different techniques is summarized in Supplementary Table 2, such as extrusion, 3D printing, and phase inversion, highlighting the excellent electrochemical performance of PCFC fabricated by extrusion technique.

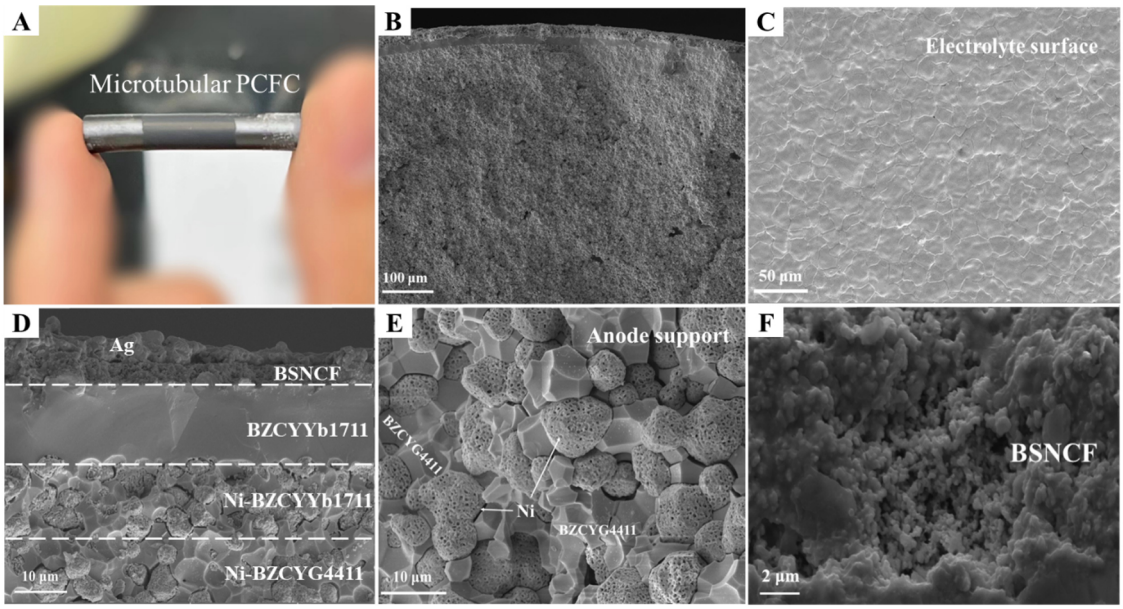

Figure 7. Structure of microtubular PCFCs. (A) Physical drawing of the microtubular PCFC; (B) the SEM cross-sectional image of the cell consisting of Ni-BZCYG4411 anode support| Ni-BZCYYb1711 functional layer|BZCYYb1711 electrolyte|cathode; (C) The electrolyte surface; (D) Typical cross-sectional SEM image of the microtubular PCFC with BSNCF; (E) The Ni-BZCYG4411 anode support after the stability test; (F) Morphology of PBSCF cathode.

Morphology of microtubular PCFC

Figure 7A shows the overall physical picture of the microtubular PCFC. The structure of PCFCs plays a crucial role in their performance and stability. As shown in Figure 7B, the three layers of the porous anode, electrolyte, and cathode remained intact and well-bonded. Figure 7C shows the surface of the electrolyte, displaying a desirable dense structure. Figure 7D shows the cross-sectional image of the microtubular PCFC with the Ni-BZCYG4411|Ni-BZCYYb1711|BZCYYb1711|BSNCF configuration after the stability test. The cell exhibits excellent structural integrity, and the dense BZCYYb1711 electrolyte effectively prevents gas leakage. The Ni-BZCYG4411 anode support is illustrated in Figure 7E, showing a uniform distribution of Ni and BZCYG4411 particles after the durability test. Finally, Figure 7F shows the morphology of BSNCF cathodes with porous structure. The large particle size might be due to high-temperature sintering during the synthesis process of SSR.

CONCLUSIONS

In this work, a novel anode-supported microtubular PCFC with a tube diameter of less than 5 mm was successfully fabricated using extrusion technology combined with dip-coating process. The microtubular PCFC exhibited good mechanical strength during testing. The newly developed BZCYG4411 proton-conducting electrolyte was synthesized using a novel one-step SSR method, showing comparable electrical conductivity with BZCYYb4411 and BZCYYb1711 electrolytes, along with excellent chemical stability in H_2O and CO_2 atmospheres. The phase structure was confirmed through XRD and TEM characterization. In addition, the single cell with BSNCF cathodes exhibited an excellent PPD of 906.86 mW cm^{-2} at 700 °C with a low R_p of 0.07 Ω cm^{-2}. Furthermore, the single cell with BSNCF cathode showed a decay rate of 3.6% after 103 h test at 650 °C. Overall, the microtubular PCFCs prepared using the extrusion technology achieved excellent electrochemical performance and stable operation. This work provides a highly efficient and simplified technology for fabricating high-performance and durable anode-supported microtubular PCFCs, with promising potential for practical applications.

DECLARATIONS

Acknowledgments

The authors acknowledge the financial support provided by the National Natural Science Foundation of China (U2005215), Anhui Province Science and Technology Major Project (202203a07020028), China Postdoctoral Science Foundation (2023M743769), and Science and Technology Program of Xuzhou (KC22017).

Authors' contributions

Conceived the research, designed the experiments and prepared cells: Zhuang, Z.; Huang, Z.
Powder synthesis and conductivity test: Zhang, X.; Liu, K.; Zheng, G.
Discussed and revised the manuscript: Chen, T.; Sun, R.; Xu, L.; Wang, S.
All authors contributed to revising the manuscript.

Availability of data and materials

Data supporting the results of this study are available from the corresponding author upon request.

Financial support and sponsorship

The work was financially supported by the National Natural Science Foundation of China (U2005215), Anhui Province Science and Technology Major Project (202203a07020028), China Postdoctoral Science Foundation (2023M743769), and Science and Technology Program of Xuzhou (KC22017).

Conflicts of interest

All authors declared that there are no conflicts of interest.

Ethical approval and consent to participate

Not applicable.

Consent for publication

Not applicable.

Copyright

© The Author(s) 2025.

REFERENCES

1. Wei, Y. M.; Chen, K.; Kang, J. N.; Chen, W.; Wang, X. Y.; Zhang, X. Policy and management of carbon peaking and carbon neutrality: a literature review. *Engineering* **2022**, *14*, 52-63. DOI
2. Shao, Z.; Ni, M. Fuel cells: materials needs and advances. *MRS. Bull.* **2024**, *49*, 451-63. DOI
3. Wang, S. Comment for the discovery of a new type of solid oxide electrolyte. *Natl. Sci. Rev.* **2017**, *4*, 285-6. DOI
4. Zhu, B.; Mi, Y.; Xia, C.; et al. A nanoscale perspective on solid oxide and semiconductor membrane fuel cells: materials and technology. *Energy. Mater.* **2022**, *1*, 100002. DOI
5. Duan, C.; Kee, R. J.; Zhu, H.; et al. Highly durable, coking and sulfur tolerant, fuel-flexible protonic ceramic fuel cells. *Nature* **2018**, *557*, 217-22. DOI
6. Vinchhi, P.; Khandla, M.; Chaudhary, K.; Pati, R. Recent advances on electrolyte materials for SOFC: a review. *Inorg. Chem. Commun.* **2023**, *152*, 110724. DOI
7. Xie, M.; Cai, C.; Duan, X.; Xue, K.; Yang, H.; An, S. Review on Fe-based double perovskite cathode materials for solid oxide fuel cells. *Energy. Mater.* **2024**, *4*, 400007. DOI
8. Yang, L.; Wang, S.; Blinn, K.; et al. Enhanced sulfur and coking tolerance of a mixed ion conductor for SOFCs: $BaZr_{0.1}Ce_{0.7}Y_{0.2-x}Yb_xO_{3-\delta}$. *Science* **2009**, *326*, 126-9. DOI
9. Wang, Y.; Ling, Y.; Wang, B.; et al. A review of progress in proton ceramic electrochemical cells: material and structural design, coupled with value-added chemical production. *Energy. Environ. Sci.* **2023**, *16*, 5721-70. DOI
10. Kim, J.; Sengodan, S.; Kim, S.; Kwon, O.; Bu, Y.; Kim, G. Proton conducting oxides: a review of materials and applications for

renewable energy conversion and storage. *Renew. Sustain. Energy. Rev.* **2019**, *109*, 606-18. DOI

11. Wang, N.; Tang, C.; Du, L.; et al. Advanced cathode materials for protonic ceramic fuel cells: recent progress and future perspectives. *Adv. Energy. Mater.* **2022**, *12*, 2201882. DOI
12. Guo, S.; Jiang, L.; Li, Y.; et al. From electrolyte and electrode materials to large-area protonic ceramic fuel cells: a review. *Adv. Funct. Mater.* **2024**, *34*, 2304729. DOI
13. Li, G.; Gou, Y.; Qiao, J.; Sun, W.; Wang, Z.; Sun, K. Recent progress of tubular solid oxide fuel cell: from materials to applications. *J. Power. Sources.* **2020**, *477*, 228693. DOI
14. Chen, R.; Gao, Y.; Gao, J.; et al. From concept to commercialization: a review of tubular solid oxide fuel cell technology. *J. Energy. Chem.* **2024**, *97*, 79-109. DOI
15. Zhang, X.; Jin, Y.; Li, D.; Xiong, Y. A review on recent advances in micro-tubular solid oxide fuel cells. *J. Power. Sources.* **2021**, *506*, 230135. DOI
16. Lawlor, V. Review of the micro-tubular solid oxide fuel cell (Part II: cell design issues and research activities). *J. Power. Sources.* **2013**, *240*, 421-41. DOI
17. Cui, D.; Cheng, M. Thermal stress modeling of anode supported micro-tubular solid oxide fuel cell. *J. Power. Sources.* **2009**, *192*, 400-7. DOI
18. Hou, M.; Zhu, F.; Liu, Y.; Chen, Y. A high-performance fuel electrode-supported tubular protonic ceramic electrochemical cell. *J. Eur. Ceram. Soc.* **2023**, *43*, 6200-7. DOI
19. Tong, G.; Li, Y.; Wang, Z.; Tan, X. Batch fabrication of micro-tubular protonic ceramic fuel cells via a phase inversion-based co-spinning/co-sintering technique. *J. Power. Sources.* **2023**, *585*, 233605. DOI
20. Liu, K.; Zhang, X.; Huang, Z.; et al. Enhancing the mass transfer of protonic ceramic fuel cells with open-straight pore structure via phase inversion tape casting. *Int. J. Hydrogen. Energy.* **2024**, *58*, 924-30. DOI
21. Chen, C.; Liu, M.; Bai, Y.; Yang, L.; Xie, E.; Liu, M. Anode-supported tubular SOFCs based on $BaZr_{0.1}Ce_{0.7}Y_{0.1}Yb_{0.1}O_{3-\delta}$ electrolyte fabricated by dip coating. *Electrochem. Commun.* **2011**, *13*, 615-8. DOI
22. Xiao, Y.; Wang, M.; Bao, D.; et al. Performance of fuel electrode-supported tubular protonic ceramic cells prepared through slip casting and dip-coating methods. *Catalysts* **2023**, *13*, 182. DOI
23. Zou, M.; Conrad, J.; Sheridan, B.; et al. 3D printing enabled highly scalable tubular protonic ceramic fuel cells. *ACS. Energy. Lett.* **2023**, *8*, 3545-51. DOI
24. Pesce, A.; Hornés, A.; Núñez, M.; Morata, A.; Torrell, M.; Tarancón, A. 3D printing the next generation of enhanced solid oxide fuel and electrolysis cells. *J. Mater. Chem. A.* **2020**, *8*, 16926-32. DOI
25. Suzuki, T.; Yamaguchi, T.; Fujishiro, Y.; Awano, M. Fabrication and characterization of micro tubular SOFCs for operation in the intermediate temperature. *J. Power. Sources.* **2006**, *160*, 73-7. DOI
26. Min, S. H.; Song, R. H.; Lee, J. G.; et al. Fabrication of anode-supported tubular $Ba(Zr_{0.1}Ce_{0.7}Y_{0.2})O_{3-\delta}$ cell for intermediate temperature solid oxide fuel cells. *Ceram. Int.* **2014**, *40*, 1513-8. DOI
27. Yang, L.; Zuo, C.; Liu, M. High-performance anode-supported solid oxide fuel cells based on $Ba(Zr_{0.1}Ce_{0.7}Y_{0.2})O_{3-\delta}$ fabricated by a modified co-pressing process. *J. Power. Sources.* **2010**, *195*, 1845-8. DOI
28. Wang, M.; Wu, W.; Lin, Y.; et al. Improved solid-state reaction method for scaled-up synthesis of ceramic proton-conducting electrolyte materials. *ACS. Appl. Energy. Mater.* **2023**, *6*, 8316-26. DOI
29. Liu, Z.; Song, Y.; Xiong, X.; et al. Sintering-induced cation displacement in protonic ceramics and way for its suppression. *Nat. Commun.* **2023**, *14*, 7984. DOI PubMed PMC
30. Zhao, Z.; Tang, S.; Liu, X.; et al. Preparation, characterization and application of $BaZr_{0.1}Ce_{0.7}Y_{0.2}O_{3-\delta}$ for a high-performance and stable proton ceramic electrochemical cell. *Int. J. Hydrogen. Energy.* **2023**, *48*, 39747-58. DOI
31. Zhou, C.; Shen, X.; Liu, D.; et al. Low thermal-expansion and high proton uptake for protonic ceramic fuel cell cathode. *J. Power. Sources.* **2022**, *530*, 231321. DOI
32. Shin, J. S.; Saqib, M.; Jo, M.; et al. Degradation mechanisms of solid oxide fuel cells under various thermal cycling conditions. *ACS. Appl. Mater. Interfaces.* **2021**, *13*, 49868-78. DOI
33. Chen, X.; Zhang, H.; Li, Y.; et al. Fabrication and performance of anode-supported proton conducting solid oxide fuel cells based on $BaZr_{0.1}Ce_{0.7}Y_{0.1}Yb_{0.1}O_{3-\delta}$ electrolyte by multi-layer aqueous-based co-tape casting. *J. Power. Sources.* **2021**, *506*, 229922. DOI
34. Zhu, L.; O'hayre, R.; Sullivan, N. P. High performance tubular protonic ceramic fuel cells via highly-scalable extrusion process. *Int. J. Hydrogen. Energy.* **2021**, *46*, 27784-92. DOI
35. Hou, M.; Pan, Y.; Chen, Y. Enhanced electrochemical activity and durability of a direct ammonia protonic ceramic fuel cell enabled by an internal catalyst layer. *Sep. Purif. Technol.* **2022**, *297*, 121483. DOI
36. Leng, Z.; Huang, Z.; Zhou, X.; et al. The effect of sintering aids on $BaCe_{0.7}Zr_{0.1}Y_{0.1}Yb_{0.1}O_{3-\delta}$ as the electrolyte of proton-conducting solid oxide electrolysis cells. *Int. J. Hydrogen. Energy.* **2022**, *47*, 33861-71. DOI
37. Lyagaeva, J.; Vdovin, G.; Hakimova, L.; Medvedev, D.; Demin, A.; Tsiakaras, P. $BaCe_{0.7}Zr_{0.1}Y_{0.1}Yb_{0.1}O_{3-\delta}$ proton-conducting electrolytes for intermediate-temperature solid oxide fuel cells. *Electrochim. Acta.* **2017**, *251*, 554-61. DOI
38. Loureiro, F. J. A.; Nasani, N.; Reddy, G. S.; Munirathnam, N. R.; Fagg, D. P. A review on sintering technology of proton conducting $BaCeO_3$-$BaZrO_3$ perovskite oxide materials for protonic ceramic fuel cells. *J. Power. Sources.* **2019**, *438*, 226991. DOI
39. Yang, K.; Wang, J. X.; Xue, Y. J.; et al. Synthesis, sintering behavior and electrical properties of $Ba(Zr_{0.1}Ce_{0.7}Y_{0.2})O_{3-\delta}$ and $Ba(Zr_{0.1}Ce_{0.7}Y_{0.1}Yb_{0.1})O_{3-\delta}$ proton conductors. *Ceram. Int.* **2014**, *40*, 15073-81. DOI

40. Luo, J.; Zhang, J.; Wang, A.; et al. Influence of particle size and sintering aid on sinterability and conductivity of $BaZr_{0.1}Ce_{0.7}Y_{0.2}O_{3-\delta}$ electrolyte. *Int. J. Hydrogen. Energy.* **2024**, *56*, 871-9. DOI
41. Huang, Z.; Yang, Y.; Lv, H.; et al. Large-area anode-supported protonic ceramic fuel cells combining with multilayer-tape casting and hot-pressing lamination technology. *J. Eur. Ceram. Soc.* **2023**, *43*, 428-37. DOI
42. Zhang, G.; Chen, T.; Guo, Z.; et al. A 10 × 10 cm^2 protonic ceramic electrochemical hydrogen pump for efficient and durable hydrogen purification. *Chem. Eng. J.* **2024**, *495*, 153521. DOI
43. Bai, H.; Chu, J.; Chen, T.; et al. $PrBa_{0.5}Sr_{0.5}Co_{1.5}Fe_{0.5}O_{5+\delta}$ as air electrode for proton-conducting solid oxide cells. *J. Power. Sources.* **2023**, *574*, 233162. DOI
44. Ullmann, H.; Trofimenko, N.; Tietz, F.; Stöver, D.; Ahmad-Khanlou, A. Correlation between thermal expansion and oxide ion transport in mixed conducting perovskite-type oxides for SOFC cathodes. *Solid. State. Ion.* **2000**, *138*, 79-90. DOI
45. Duan, C.; Hook, D.; Chen, Y.; Tong, J.; O'hayre, R. Zr and Y co-doped perovskite as a stable, high performance cathode for solid oxide fuel cells operating below 500 °C. *Energy. Environ. Sci.* **2017**, *10*, 176-82. DOI
46. Wang, Z.; Lv, P.; Yang, L.; et al. $Ba_{0.95}La_{0.05}Fe_{0.8}Zn_{0.2}O_{3-\delta}$ cobalt-free perovskite as a triple-conducting cathode for proton-conducting solid oxide fuel cells. *Ceram. Int.* **2020**, *46*, 18216-23. DOI
47. Lv, X.; Chen, H.; Zhou, W.; Li, S.; Shao, Z. A CO_2-tolerant $SrCo_{0.8}Fe_{0.15}Zr_{0.05}O_{3-\delta}$ cathode for proton-conducting solid oxide fuel cells. *J. Mater. Chem. A.* **2020**, *8*, 11292-301. DOI
48. Cao, D.; Zhou, M.; Yan, X.; Liu, Z.; Liu, J. High performance low-temperature tubular protonic ceramic fuel cells based on barium cerate-zirconate electrolyte. *Electrochem. Commun.* **2021**, *125*, 106986. DOI
49. Zhou, C.; Wang, X.; Liu, D.; et al. New strategy for boosting cathodic performance of protonic ceramic fuel cells through incorporating a superior hydronation second phase. *Energy. Environ. Mater.* **2024**, *7*, e12660. DOI
50. Zhang, Y.; Chen, Y.; Yan, M.; Chen, F. Reconstruction of relaxation time distribution from linear electrochemical impedance spectroscopy. *J. Power. Sources.* **2015**, *283*, 464-77. DOI
51. Zhao, Y.; Zhang, K.; Wei, Z.; et al. Performance and distribution of relaxation times analysis of Ruddlesden-Popper oxide $Sr_3Fe_{1.3}Co_{0.2}Mo_{0.5}O_{7-\delta}$ as a potential cathode for protonic solid oxide fuel cells. *Electrochim. Acta.* **2020**, *352*, 136444. DOI
52. Xia, J.; Wang, C.; Wang, X.; Bi, L.; Zhang, Y. A perspective on DRT applications for the analysis of solid oxide cell electrodes. *Electrochim. Acta.* **2020**, *349*, 136328. DOI
53. Sumi, H.; Shimada, H.; Yamaguchi, Y.; Yamaguchi, T.; Fujishiro, Y. Degradation evaluation by distribution of relaxation times analysis for microtubular solid oxide fuel cells. *Electrochim. Acta.* **2020**, *339*, 135913. DOI
54. Li, G.; Gou, Y.; Ren, R.; et al. Fluorinated $Pr_2NiO_{4+\delta}$ as high-performance air electrode for tubular reversible protonic ceramic cells. *J. Power. Sources.* **2021**, *508*, 230343. DOI
55. Kuroha, T.; Yamauchi, K.; Mikami, Y.; et al. Effect of added Ni on defect structure and proton transport properties of indium-doped barium zirconate. *Int. J. Hydrogen. Energy.* **2020**, *45*, 3123-31. DOI